

Architecture Engineering of One Body Nanostructured Catalyst: Layer-By-Layer Adornment of Multiple Nanocatalysts On Silica Nanorod Arrays For Hydrogenation of Nitroarenes

Kootak Hong

Seoul National University

Jun Min Suh

Seoul National University

Tae Hyung Lee

Seoul National University

Seeram Ramakrishna

National University of Singapore

Rajender S. Varma

Palacký University

Ho Won Jang

Seoul National University

Mohammadreza Shokouhimehr (✉ mrsh2@snu.ac.kr)

Seoul National University

Research Article

Keywords: Catalysis, Nanostructure, Hydrogenation, Reduction, Coupling reaction

Posted Date: July 7th, 2021

DOI: <https://doi.org/10.21203/rs.3.rs-658873/v1>

License:   This work is licensed under a Creative Commons Attribution 4.0 International License.

[Read Full License](#)

Abstract

Direct consideration for both, the catalytically active species and the host materials provides highly efficient strategies for the architecture design of nanostructured catalysts. The conventional wet chemical methods have limitations in achieving such unique layer-by-layer design possessing one body framework with many catalyst parts. Herein, an innovative physical method is presented that allows the well-regulated architecture design for an array of functional nanocatalysts as exemplified by layer-by-layer adornment of Pd nanoparticles (NPs) on the highly arrayed silica nanorods. This spatially confined catalyst exhibits excellent efficiency for the hydrogenation of nitroarenes and widely deployed Suzuki cross-coupling reactions; their facile separation from the reaction mixtures is easily accomplished due to the monolithic structure. The generality of this method for the introduction of other metal source has also been demonstrated with Au NPs. This pioneering effort highlights the feasibility of physically controlled architecture design of nanostructured catalysts which may stimulate further studies in the general domain of the heterogeneous catalytic transformations.

Introduction

Catalysts are sine qua non for most of the chemical processes to produce fine chemicals, pharmaceuticals, petrochemicals, among plethora of other fine chemicals.¹⁻⁷ From the industrial point of view, heterogeneous catalysts are often preferred to their homogeneous counterparts because of low cost, easy separation from reaction mixture, stability, and reusability.⁸⁻¹⁰ In addition, the use of heterogeneous catalysts in continuous flow processes have several advantageous features such as easy mass production, automation, higher yields, and quality of products.¹¹⁻¹⁴

Despite these remarkable advantages, one of the critical issues in heterogeneous catalysts is their low catalytic activity and selectivity.¹⁵⁻¹⁷ In particular, very low catalytic activity and the rapid decay in efficiency are inevitable when they are stabilized in the non-porous solid supports. Therefore, chemical and material engineers have made several strides to design and synthesize heterogeneous catalysts with enhanced catalytic activity and selectivity. As supported heterogeneous catalysts are composed of two important segments: (i) catalytically active metal nanoparticles (NPs), and (ii) support materials.¹⁸⁻²⁰, the developed methodologies to enhance the catalytic activity of metal NPs entails tailoring their morphologies, facets, and atomic arrangements.²¹⁻²⁴ Support materials have also been extensively developed to uncover facile recyclability, good physiochemical stability, high surface area for the accessibility of metal nanocatalysts to various substrates and reactants.²⁵⁻²⁸ In addition, various approaches have been explored to functionalize the engineered heterogeneous catalysts thus enabling them to accommodate high loading capacity of catalytically active nanocatalysts and ameliorating their performance.²⁹⁻³⁴

For the next generation of heterogeneous catalysts endowed with specific functions and high catalytic activity, it is indispensable to design the architecture of engineered catalytically active NPs to be

deposited in the accessible positions. Undeniably, the catalytic systems often developed by wet chemistry, the widely used method to prepare heterogeneous catalysts, cannot immobilize multiple catalytically active NPs on supports in a controllable manner at the designed nanoscale.^{35–38} Even if endeavored, it requires very complicated and time-consuming multi-step process and the deployment of toxic chemical reagents. Therefore, new methods of designing and fabricating the heterogeneous catalysts comprising unique frameworks with various components should be planned.

Physically controlled decoration of catalytically active species on certain well-known and defined supports provides a great potential to fulfill this objective. Compared to the conventional wet-chemical methods, this strategy presents advantages of well-tolerated loading amounts and decoration locations on supports, which is unattainable by existing synthetic techniques. Consequently, we established in our approach the highly tolerable design of benign hosts and catalytically active species.

A novel template-free and designable bottom-up grown Pd NPs deposited on vertically aligned SiO₂ nanorod arrays (v-SiO₂ NRs@Pd) nanostructured catalyst (prepared by glancing angle deposition (GLAD) method) is reported for the reduction of nitroarenes. Due to shadowing effect during the GLAD process, SiO₂ NRs can be deposited on silicon wafers. As SiO₂ NRs have top open structure, accessible Pd NPs can be precisely decorated on the surface of SiO₂ NRs in a layer-by-layer architecture benefitting from a multiple-step GLAD method. Furthermore, our strategy enables the combinations of various metal NPs and support materials, and nano-scale controlled affixation of catalyst NPs robustly on nanorod arrays.

Materials And Methods

Oxide grains (SiO₂ and SnO₂) and metal pellets (Pd and Au) with 99.99 % purity, used for film deposition, were purchased from Kojundo Chemistry. The other chemicals used in this study were purchased from the Daejung and Samchun Chemical Companies.

Fabrication of the v-SiO₂ NRs@Pd nanostructured catalyst: A *p*-type Si wafers were cleaned in acetone, isopropanol, and deionized water under ultrasonication followed by drying in a nitrogen atmosphere. To make SiO₂ NRs, the evaporation was performed at a glancing angle with a rotation speed of 40 rpm; the wafer was located 50 cm away from the crucible, tilted at 80°. The base pressure was maintained at 1.0×10^{-6} Torr and growth rate was 1.0 \AA s^{-1} . After 250 nm-thick SiO₂ NRs deposition, 3 nm-thick Pd film was sequentially deposited on the wafer at the original position (0°). These processes were repeatedly carried out until the 1 μm -thick v-SiO₂ NRs were obtained. All the fabricated catalysts were annealed at 300°C for 30 minutes in a reducing atmosphere.

The morphology of the v-SiO₂ NRs@Pd nanostructure catalyst was characterized using a field-emission scanning electron microscopy (FESEM, Zeiss SUPRA 55VP). The transmission electron microscopy (TEM) and cross-sectional high-resolution TEM images were obtained using a 200 kV field-emission TEM (JEM-2100 F, JEOL). A focused ion beam (FIB, Helios 650) was utilized to prepare the samples for TEM analysis. The energy-dispersive X-ray spectroscopy (EDS) analysis was conducted to investigate the

chemical mapping of the v-SiO₂ NRs@Pd nanostructured catalyst. Grazing-incidence X-ray powder diffraction (GIXRD) was performed using PANalytical X'pert Pro X-ray diffractometer. The X-ray photoelectron spectroscopy (XPS) was carried out using AXIS Ultra DLD instrument (Kratos, U.K.) operating at a base pressure of 1.6×10^{-10} mbar at 300 K. An inductively coupled plasma atomic emission spectrometer (ICP-AES, Varian 730ES) was used for the measurement of Pd amount. The products from the catalytic reactions were analyzed by a gas chromatography mass spectrometer (GC-MS) using an Agilent Technologies 7693 Autosampler. The structures of the chemical products were identified using a nuclear magnetic resonance (NMR, 600MHz, High Resolution NMR Spectrometer, AVANCE Bruker).

Results And Discussion

The fabrication process for the v-SiO₂ NRs@Pd nanostructured catalyst using an electron beam evaporator is illustrated in Fig. 1. A multiple-step GLAD was utilized to deposit v-SiO₂ NRs on a *p*-type Si wafer and effectively adorning Pd NPs on v-SiO₂ NRs, substantially improving the previously reported methods.³⁹⁻⁴¹ SiO₂ was deposited on a *p*-type Si wafer tilted at 80° and rotated with a speed of 80 rpm. After deposition of a 250 nm-thick layer of SiO₂ NRs, a 3 nm-thick Pd layer was deposited at a tilt angle of 0° on the v-SiO₂ NRs. These steps were performed repeatedly until the total length of the v-SiO₂ NRs reached to 1 μm. Finally, the fabricated catalysts were annealed at 300°C under a reducing atmosphere to furnish robustly stabilized Pd NPs.

As shown in Fig. 2a and b, v-SiO₂ NRs@Pd nanostructured catalyst was uniformly deposited on 4-inch Si wafer. The cross-sectional scanning electron microscopy image in Fig. 2b shows highly one-dimensional structures of v-SiO₂ NRs@Pd catalyst on the Si wafer substrate. The nanorods were separated from each other by elongated pores and their average diameter was about 60 nm, improving the approachability of the Pd NPs and diffusion of the reactants and products. Due to their accessible nanostructure, reagents can efficiently permeate into and interact with the v-SiO₂ NRs@Pd nanostructured catalyst. To clarify the existence of Pd NPs in the v-SiO₂ NRs, GIXRD was performed which revealed the peaks assignable to the (111) and (200) reflections of the face-centered cubic (FCC) Pd NPs (Fig. 2c). XPS analysis was also carried out to confirm the oxidation state of Pd species in v-SiO₂ NRs@Pd nanostructured catalyst (Fig. 2d). The peaks corresponding to Si, O, and Pd are clearly observed in XPS spectra (Fig. S1). The Pd 3d_{5/2} and Pd 3d_{3/2} binding energies were found to be at 335.8 and 341.1 eV, respectively thus indicating the formation of zero-valent Pd species in v-SiO₂ NRs@Pd nanostructured catalyst.

To further analyze the nanostructured of v-SiO₂ NRs@Pd catalyst, TEM images were obtained as shown in Fig. 3a; four dense layers of Pd NPs were seen clearly deposited on v-SiO₂ NRs. The Pd NPs were also observed in the side walls of the v-SiO₂ NRs. The energy dispersive spectroscopy (EDS) mapping on the v-SiO₂ NRs@Pd nanostructured catalyst was conducted. Figure 3b-d show the chemical mapping images of Si, O, and Pd elements for the selected areas in Fig. 3a (orange dashed rectangle). For Si and O

elements, a uniform distribution across the v-SiO₂ NRs has been observed. However, Pd NPs were distributed in a layer-by-layer architecture with total of four layers. The Pd element observed in between the layers has been attributed to the Pd NPs on sidewalls of v-SiO₂ NRs. Figure 3e–g shows the high resolution TEM (HRTEM) images of Pd NPs on the surface (yellow rectangle) of the SiO₂ NRs; Pd NPs were crystallized with the (111) preferred orientation. From the above results, it can be concluded that Pd NPs are efficiently decorated on the whole surface area of SiO₂ NRs and immobilized at desired locations on SiO₂ NRs through multiple-step GLAD method to realize a favorable spatial confinement. In other words, the catalytic active sites, Pd NPs, are well-refined on the v-SiO₂ NR supports, resulting in more accessible catalytically active sites on the v-SiO₂ NRs@Pd nanostructured catalyst.

To further demonstrate the advantages of this physical architecture design, we fabricated v-SiO₂ NRs decorated with Au and Pd alternately (v-SiO₂ NRs@Pd/Au), using the same protocol. The four dense layers of metal NPs were observed on the v-SiO₂ NRs@Pd/Au nanostructured catalyst (Fig. S2). The EDS mapping on the v-SiO₂ NRs@Pd/Au nanostructured catalyst revealed that the Pd and Au NPs were layer-by-layer deposited on v-SiO₂ NRs by turns. The HRTEM images also confirmed that the metal NPs were single crystalline in each layer for both, the Au and Pd NPs.

To confirm the oxidation state of Pd and Au NPs, XPS analysis was conducted. The peaks observed at 84.1, 87.8, 335.8, and 341.2 eV corresponded to Au 4f_{7/2}, Au 4f_{5/2}, Pd 3d_{5/2} and Pd 3d_{3/2}, respectively. This indicated that the Pd and Au NPs on the v-SiO₂ NRs@Pd/Au nanostructured catalyst were in zero-valent state. The similar catalyst was also synthesized on SnO₂ supports using our strategy to broaden various type of supporting materials. As shown in Fig. S3, Pd NPs were well-decorated on v-SnO₂ NRs. These results illustrated that metal NPs could be stabilized on the designed sites on various supports using the multiple-step GLAD physical method.

Compared with previously reported fabrication processes for nanostructured catalysts, this approach has several advantages including favorable design, precise architecture engineering, and accessible metal nanocatalysts for the reactants, *etc.*^{42–44} Using wet chemical methods, mainly applied for nanostructured catalysts fabrication, catalytic sites are randomly distributed due to the lack of controllability and the need for complicated functionalization processes.⁴⁵ In addition, it is very difficult to combine two or more metal NPs into the nanostructured support. However, this approach circumvents the limitations of previous reports for the catalysts on silicon wafers as the supporting materials via top-down fabrication process often is accompanied by harmful and toxic HF etching.⁴⁶ The present strategy provides the varying catalytically active sites precisely integrated on the support and their location can be controlled on nanoscale, thus improving the approachability of the catalytic NPs to reactants.

To verify the catalytic activity and chemoselectivity of the v-SiO₂ NRs@Pd nanostructured catalyst, we conducted the hydrogenation of various substituted nitroaromatics at room temperature; a reaction that has important impact in many industries, including environmental safety.^{47–50} Our designed

nanostructured catalyst presented superb catalytic activity for the selective hydrogenation of nitroaromatics in aqueous solution (Table 1). The procedure was accomplished under eco-friendly mild conditions, attaining high yields for the hydrogenation of substituted nitroaromatics to the corresponding aminoaromatics. The hydrogenation of nitroaromatics bearing two reducible groups could be achieved selectively to the amino moiety as the only product, while another reducible group was retained unchanged (Table 1, entries 4–6). In addition, achieving highly selective reduction of nitro groups of aromatic molecules possessing olefin bonds is very challenging as there is high probability for both the functional groups to be readily hydrogenated. Importantly, this process proceeded with high selectivity (99%), reducing only nitro group (Table 1, entry 8) as affirmed by nuclear magnetic resonance spectroscopy (Fig. S4).

To clarify the correlation between accessibility of Pd nanocatalysts and their activity, as a proof-of-concept, control experiments were carried out using various nanostructured catalysts in the hydrogenation of nitrobenzene as a model reaction under identical reaction conditions (Table S1). Initially, only Pd NPs were deposited on silicon wafer by GLAD method aiming for simple recycling through dipping and removing of the silicon substrate possessing stable nanocatalysts. The reaction produced a low yield of (15%) of aniline under optimized reaction conditions. FESEM images of this catalyst showed that the surface of the silicon wafer substrate was thoroughly covered by stacked Pd NPs without approachable opening for the diffusion of the reactants, resulting in low catalytic activity (Fig. S5). In addition, micro- and nano-space channels provide permeable paths to organic reagents, thus improving the accessibility of the Pd nanocatalysts.^{51–53} We also fabricated and evaluated the catalytic activity of Pd NPs on SiO₂ arrays having ~ 200 nm height (Fig. S6). Interestingly, the SiO₂ columns exposing Pd NPs could hydrogenate the nitro group of nitrobenzene in relatively higher yields (35%). Although the prototype short length SiO₂ arrays were partly aggregated, from this result we found that the Pd NPs stabilized on sturdy SiO₂ support functioned to some extent effectively, which can be attributed to internal surface and pore diffusivity.⁵⁴ Consequently, we designed and fabricated SiO₂ arrays and aligning them separately from each other with ~ 600 nm length possessing Pd NPs on their scaffolds as depicted in FESEM image (Fig. S7). Although the Pd NPs were located irregularly on the SiO₂ arrays, their combination improved their interactions with the solvent and reactants via the accessible pores, promoting efficient catalytic reactions (Table S1, entry 3). Finally, we designed and developed fully arranged and assorted v-SiO₂ NRs@Pd catalyst having permeable tunnel nanostructure and elongated pores between SiO₂ columns with four strata of attainable Pd NPs, and maximizing their catalytic activity in the given geometric configuration. Similarly, the alternatively four dense layers of Pd NPs and Au NPs in the v-SiO₂ NRs@Pd/Au nanostructured catalyst provided high catalytic activity in the model reduction. The combination and the activity of different nanocatalysts can easily be tuned and optimized by this method, controlling their locations on supports and distance between the nanocatalysts and the arrays. The controlled pores in the nanostructure provided facile adsorption of reactants to the Pd NPs and subsequent desorption of products from them. Additionally, a larger amount of Pd NPs can be decorated on the whole surface of SiO₂ NRs exposing large amount of accessible Pd sites for the catalytic

reactions. Thus, v-SiO₂ NRs@Pd nanostructured catalyst could expedite Suzuki coupling reaction of various aryl halides with phenylboronic acid (Table 2); reaction of aryl iodides and aryl bromides with phenylboronic acid proceeded with excellent conversion in 3 h and 5 h, respectively.

Recycling and reuse of the catalysts are crucial parameters because of the environmental impact and practical applications. Although many heterogeneous catalysts have been developed for the reduction of nitroaromatics, they generally entail very arduous recycling procedures such as centrifugation, filtration, laborious work-up purification, *etc.* However, v-SiO₂ NRs@Pd nanostructured catalyst could be easily separated being withdrawn from the reaction mixture by tweezers, as they have a monolithic structure, a salient advantage of our catalyst. The durability and reusability of our catalyst was investigated for the hydrogenation of nitrobenzene. After completion of the reaction, the v-SiO₂ NRs@Pd nanostructured catalyst was simply removed from the reaction mixture, rinsed with water, and reused in the next cycle. The activity of the catalyst remained stable even after seven consecutive reaction cycles, though there was a minuscule decline in activity of the catalyst (Table 3). As the catalytic activity of v-SiO₂ NRs@Pd nanostructured catalyst originates from its special architecture engineering of one body nanostructure, we precisely characterized the recovered v-SiO₂ NRs@Pd nanostructured catalyst by EDX, TEM, and HRTEM techniques (Fig. S8), affirming the constant stability of the designed catalyst after the recycling. Consequently, Pd leaching could be the reason for this catalytic decrease, which was supported by ICP-AES analysis; negligible Pd species (0.04 mg L⁻¹) was detected.

Conclusions

The novel synthesis of v-SiO₂ NRs@Pd nanostructured catalyst described in this study exhibited promising catalytic characteristics for the hydrogenation of nitroaromatics and the Suzuki cross-coupling reaction. The vertically aligned SiO₂ NRs provided an excellent platform for Pd nanocatalysts to be firmly cohered to create a monolithic structure, which is superior in the realization of a simple recycling process. Because this fabrication procedure is based on physical vapor deposition under vacuum conditions, it can be applied to various combinations of metal nanocatalysts and supporting nanostructures without complicated synthesis procedures often deployed in wet chemical methods. The effective design of nano-architectures for a monolithic nanocatalysts-attached SiO₂ NRs will expectedly open new perspectives toward the development of highly recyclable nanocatalysts for other catalytic reactions.

Declarations

Acknowledgements

This research was supported by National Research Foundation of Korea (NRF) funded by the Ministry of Science and ICT (2020M2D8A206983011). Furthermore, the financial supports of the Basic Science

Research Program (2017R1A2B3009135) through the National Research Foundation of Korea is appreciated.

Conflict of interest

The authors declare no conflict of interest.

References

1. Hagen, J. *Industrial catalysis: a practical approach* (John Wiley & Sons, 2015).
2. Ross, J. R. *Heterogeneous catalysis: fundamentals and applications* (Elsevier, 2011).
3. Polshettiwar, V. & Varma, R. S. Green chemistry by nano-catalysis. *Green Chem*, **12**, 743–754 (2010).
4. Polshettiwar, V., Baruwati, B. & Varma, R. S. Self-Assembly of Metal Oxides into Three-Dimensional Nanostructures: Synthesis and Application in Catalysis. *ACS Nano*, **3**, 728–736 (2009).
5. Ji, D. *et al.* Thin MoS₂ nanosheets grafted MOFs-derived porous Co–N–C flakes grown on electrospun carbon nanofibers as self-supported bifunctional catalysts for overall water splitting. *J. Mater. Chem. A*, **5**, 23898–23908 (2017).
6. Huang, W. *et al.* Highly Active Heterogeneous Palladium Nanoparticle Catalysts for Homogeneous Electrophilic Reactions in Solution and the Utilization of a Continuous Flow Reactor. *J. Am. Chem. Soc.*, **132**, 16771–16773 (2010).
7. Liu, L. & Corma, A. Metal Catalysts for Heterogeneous Catalysis: From Single Atoms to Nanoclusters and Nanoparticles. *Chem. Rev.*, **10**, 4981–5079 (2018).
8. Cui, X., Li, W., Ryabchuk, P., Junge, K. & Beller, M. Nanostructuring unlocks high performance of platinum single-atom catalysts for stable vinyl chloride production. *Nat. Catal.*, **1**, 376–385 (2020).
9. White, R. J., Luque, R., Budarin, V. L., Clark, J. H. & Macquarrie, D. J. Supported metal nanoparticles on porous materials. *Methods and applications. Chem. Soc. Rev.*, **38**, 481–494 (2009).
10. Wang, Z. L., Li, C. & Yamauchi, Y. Nanostructured nonprecious metal catalysts for electrochemical reduction of carbon dioxide. *Nano Today*, **11**, 373–391 (2016).
11. Bavykina, A., Kolobov, N., Khan, I. S., Bau, J. A. & Ramirez, Gascon, J. Metal–Organic Frameworks in Heterogeneous Catalysis: Recent Progress, New Trends, and Future Perspectives. *Chem. Rev.*, **120**, 8468–8535 (2020).
12. Goetjen, T. A. *et al.* Metal–organic framework (MOF) materials as polymerization catalysts: a review and recent advances. *Chem. Commun.*, **56**, 10409–10418 (2020).
13. Fan, Z. & Zhang, H. Crystal phase-controlled synthesis, properties and applications of noble metal nanomaterials. *Chem. Soc. Rev.*, **45**, 63–82 (2016).
14. Hulsey, M. J., Lim, C. W. & Yan, N. Promoting heterogeneous catalysis beyond catalyst design. *Chem. Sci.*, **11**, 1456–1468 (2020).

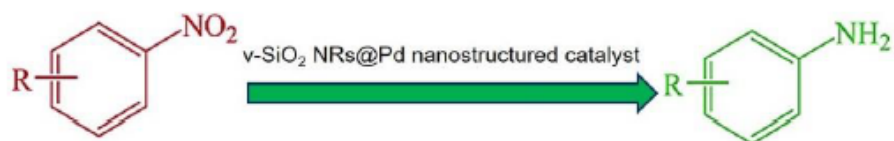
15. Mahmoud, M. A., Narayanan, R. & El-Sayed, M. A. Enhancing Colloidal Metallic Nanocatalysis: Sharp Edges and Corners for Solid Nanoparticles and Cage Effect for Hollow Ones. *Acc. Chem. Res*, **46**, 1795–1805 (2013).
16. Bakhtiarzadeh, Z. *et al.* Hydrothermal self - sacrificing growth of polymorphous MnO₂ on magnetic porous-carbon (Fe₃O₄@Cg/MnO₂): A sustainable nanostructured catalyst for activation of molecular oxygen. *Mol. Catal*, **509**, 111603 (2021).
17. Gawande, M. B., Branco, P. S. & Varma, R. S. Nano-magnetite (Fe₃O₄) as a support for recyclable catalysts in the development of sustainable methodologies. *Chem. Soc. Rev*, **42**, 3371–3393 (2013).
18. Polshettiwar, V. *et al.* *Magnetically Recoverable Nanocatalysts*. *Chem. Rev*, **111**, 3036–3075 (2011).
19. Zaera, F. Nanostructured materials for applications in heterogeneous catalysis. *Chem. Soc. Rev*, **42**, 2746–2762 (2013).
20. Shokouhimehr, M., Shahedi Asl, M. & Mazinani, B. Modulated large-pore mesoporous silica as an efficient base catalyst for the Henry reaction. *Res. Chem. Intermed*, **44**, 1617–1626 (2018).
21. Astruc, Q. W. D. State of the Art and Prospects in Metal–Organic Framework (MOF)-Based and MOF-Derived Nanocatalysis. *Chem. Rev*, **120**, 1438–1511 (2020).
22. Perego, C. & Millini, R. Porous materials in catalysis: challenges for mesoporous materials. *Chem. Soc. Rev*, **42**, 3956–3976 (2013).
23. Ishida, T., Murayama, T., Taketoshi, A. & Haruta, M. Importance of Size and Contact Structure of Gold Nanoparticles for the Genesis of Unique Catalytic Processes. *Chem. Rev*, **120**, 464–525 (2020).
24. Hu, H. *et al.* Synthesis and stabilization of metal nanocatalysts for reduction reactions-a review. *J. Mater. Chem. A*, **3**, 11157–11182 (2015).
25. Hong, K. *et al.* Palladium nanoparticles on assorted nanostructured supports: applications for Suzuki, Heck, and Sonogashira cross-coupling reactions. *ACS Appl. Nano Mater*, **3**, 2070–2103 (2020).
26. Shi On the Synergetic Catalytic Effect in Heterogeneous Nanocomposite Catalysts. *Chem. Rev*, **113**, 2139–2181 (2013).
27. Verma, P., Kuwahara, Y., Mori, K., Raja, R. & Yamashita, H. Functionalized mesoporous SBA-15 silica: recent trends and catalytic applications. *Nanoscale*, **12**, 11333–11363 (2020).
28. Sogut, E. G., Kuyuldar, H. A., karatas, Y., Gulcan, M. & Sen, F. Single-walled carbon nanotube supported Pt-Ru bimetallic superb nanocatalyst for the hydrogen generation from the methanolysis of methylamine-borane at mild conditions. *Sci. Rep*, **9**, 15724 (2019).
29. Zhang, K. *et al.* Pd modified prussian blue frameworks: Multiple electron transfer pathways for improving catalytic activity toward hydrogenation of nitroaromatics. *Mol. Catal*, **492**, 110967 (2020).
30. Favier, I., Pla, D. & Gómez, M. Palladium Nanoparticles in Polyols: Synthesis, Catalytic Couplings, and Hydrogenations. *Chem. Rev*, **120**, 1146–1183 (2020).
31. Tao, R. *et al.* Porous organic polymer material supported palladium nanoparticles. *J. Mater. Chem. A*, **8**, 17360–17391 (2020).

32. Easson, M. W., Jordan, J. H., Bland, J. M., Hinchliffe, D. J. & Condon, B. D. Application of Brown Cotton-Supported Palladium Nanoparticles in Suzuki–Miyaura Cross-Coupling Reactions. *ACS Appl. Nano Mater*, **3**, 6304–6309 (2020).
33. Li, Z. *et al.* Well-Defined Materials for Heterogeneous Catalysis: From Nanoparticles to Isolated Single-Atom Sites. *Chem. Rev*, **120**, 623–682 (2020).
34. Wang, C., Wang, Q., Fu, F. & Astruc, D. Hydrogen Generation upon Nanocatalyzed Hydrolysis of Hydrogen-Rich Boron Derivatives: Recent Developments. *ACC. Chem. Res*, **53**, 2483–2493 (2020).
35. Yang, N. *et al.* *Adv. Mater*, **30**, 1803234 (2018).
36. Zhan, G., Li, P. & Zeng, H. C. Architectural Designs and Synthetic Strategies of Advanced Nanocatalysts. *Adv. Mater*, **30**, 1802094 (2018).
37. Shokouhimehr, M. *et al.* Magnetically retrievable nanocomposite adorned with Pd nanocatalysts: efficient reduction of nitroaromatics in aqueous media. *Green Chem*, **20**, 3809–3817 (2018).
38. Shokouhimehr, M. Magnetically separable and sustainable nanostructured catalysts for heterogeneous reduction of nitroaromatics. *Catalysts*, **5**, 534 (2015).
39. Jeon, J. M. *et al.* Vertically ordered SnO₂ nanobamboos for substantially improved detection of volatile reducing gases. *J. Mater. Chem. A*, **3**, 17939–17945 (2015).
40. Sanchez-Valencia, J. R., Longtin, R., Rossell, M. D. & Gröning, P. Growth Assisted by Glancing Angle Deposition: A New Technique to Fabricate Highly Porous Anisotropic Thin Films. *ACS Appl. Mater. Interfaces*, **8**, 8686–8693 (2016).
41. Barranco, A., Borrás, A., Gonzalez-Elipe, A. R. & Palmero, A. Perspectives on oblique angle deposition of thin films: From fundamentals to devices. *Prog. Mater. Sci*, **76**, 59–153 (2016).
42. Yang, X. *et al.* Highly efficient reusable catalyst based on silicon nanowire arrays decorated with copper nanoparticles. *J. Mater. Chem. A*, **2**, 9040–9047 (2014).
43. Katal, R. *et al.* Pd-Decorated CuO Thin Film for Photodegradation of Acetaminophen and Triclosan under Visible Light Irradiation. *Adv. Mater. Interfaces*, **5**, 1801440 (2018).
44. Jin, Z., Liu, C., Qi, K. & Cui, X. Photo-reduced Cu/CuO nanoclusters on TiO₂ nanotube arrays as highly efficient and reusable catalyst. *Sci. Rep*, **7**, 39695 (2017).
45. Goswami, A. *et al.* Pt nanoparticles decorated TiO₂ nanotubes for the reduction of olefins. *Appl. Mater. Today*, **10**, 86–92 (2018).
46. Yamada, Y. M. A., Yuyama, Y., Sato, T., Fujikawa, S. & Uozumi, Y. A Palladium-Nanoparticle and Silicon-Nanowire-Array Hybrid: A Platform for Catalytic Heterogeneous Reactions. *Angew. Chem. Int. Ed*, **53**, 127–131 (2014).
47. Shokouhimehr, M., Lee, J. E., Han, S. I. & Hyeon, T. Magnetically recyclable hollow nanocomposite catalysts for heterogeneous reduction of nitroarenes and Suzuki reactions. *Chem. Commun*, **49**, 4779–4781 (2013).
48. Nayebi, B. *et al.* Boron nitride-palladium nanostructured catalyst: efficient reduction of nitrobenzene derivatives in water. *Nano express*, **1**, 030012 (2020).

49. Shokouhimehr, M., Mahmoudi Gom-Yek, S., Nasrollahzadeh, M., Kim, A. & Varma, R. S. Palladium nanocatalysts on hydroxyapatite: green oxidation of alcohols and reduction of nitroarenes in water. *Appl. Sci*, **9**, 4183 (2019).
50. Kadam, H. K. & Tilve, S. G. Advancement in methodologies for reduction of nitroarenes. *RSC Adv*, **5**, 83391–83407 (2015).
51. Shokouhimehr, M. *et al.* Magnetically recyclable core–shell nanocatalysts for efficient heterogeneous oxidation of alcohols. *J. Mater. Chem. A*, **2**, 7593–7599 (2014).
52. kalantari, E., Khalilzadeh, M. A., Zareyee, D. & Shokouhimehr, M. Catalytic degradation of organic dyes using green synthesized Fe₃O₄-cellulose-copper nanocomposites. *J. Mol. Struct*, **1218**, 128488 (2020).
53. Cheng, T., Zhang, D., Li, H. & Liu, G. Magnetically recoverable nanoparticles as efficient catalysts for organic transformations in aqueous medium. *Green Chem*, **16**, 3401–3427 (2014).
54. Iwamoto, M., Tanaka, Y., Sawamura, N. & Namba, S. Remarkable Effect of Pore Size on the Catalytic Activity of Mesoporous Silica for the Acetalization of Cyclohexanone with Methanol. *J. Am. Chem. Soc*, **125**, 13032–13033 (2003).

Tables

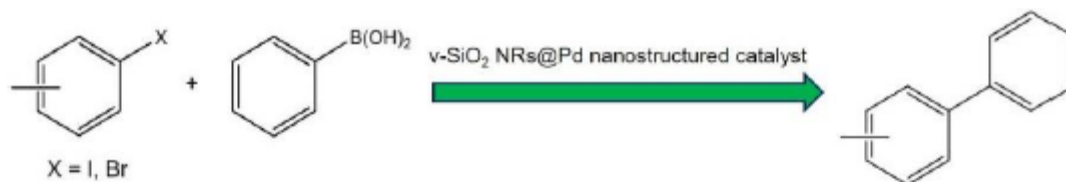
Table 1. Heterogeneous reduction of substituted nitroarenes catalyzed by v-SiO₂ NRs@Pd nanostructured catalyst.



Entry	Substrate	Product	Yields (%) ^a
1			99
2			92
3			93
4			91
5			94
6			92
7			95
8			94

Reaction conditions: Substituted nitroarenes (0.1 mmol), NaBH₄ (0.12 mmol), v-SiO₂ NRs@Pd nanostructured catalyst (1 mol% Pd), H₂O (20 mL), room temperature, and 1.5 h. ^a Yields were determined by GC-MS.

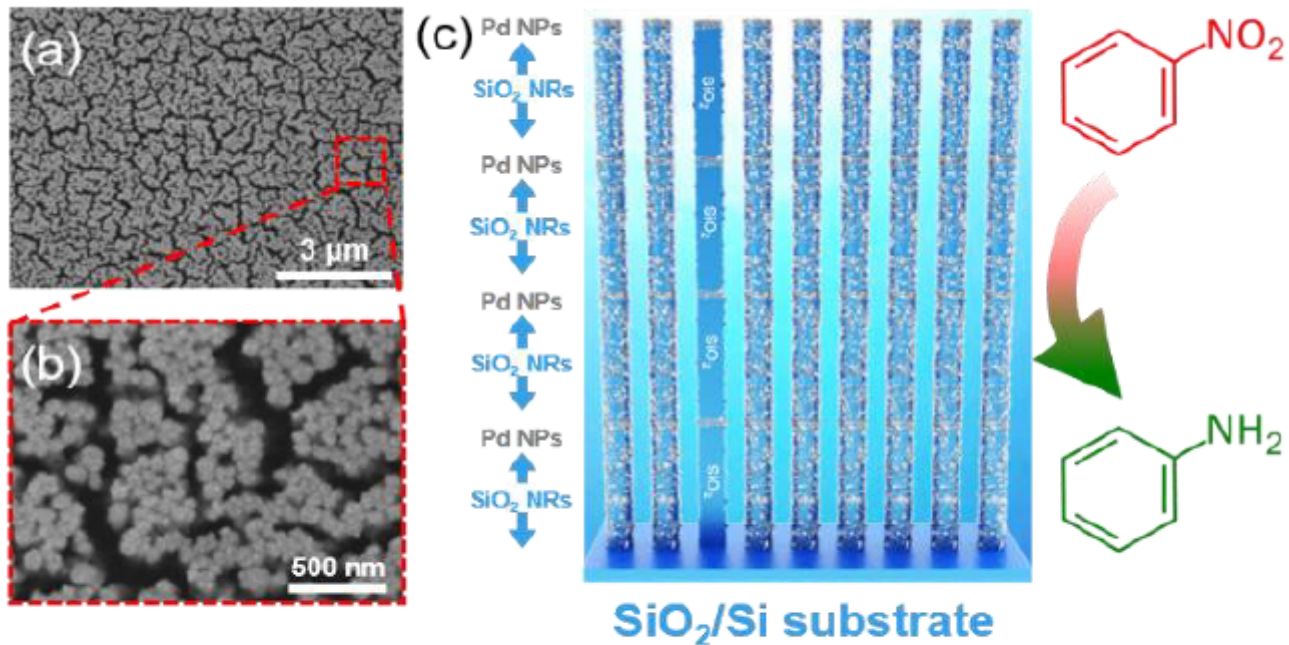
Table 2. Suzuki cross-coupling reactions catalyzed by v-SiO₂ NRs@Pd nanostructured catalyst.



Entry	Substrate	Time (h)	Yields (%) ^a
1		3	97
2		3	94
3		5	95
4		5	91
5		5	87

Reaction conditions: Aryl halide (0.1 mmol), phenylboronic acid (0.12 eq.), v-SiO₂ NRs@Pd nanostructured catalyst (1 mol%), K₂CO₃ (1.5 eq.), DMF/H₂O (5:1), 100 °C. ^aYields were determined by GC-MS.

Table 3. Reuse of v-SiO₂ NRs@Pd nanostructured catalyst in the heterogeneous reduction of nitrobenzene.



Cycle number	1	2	3	4	5	6	7
Yield of product (%) ^a	99	97	93	90	88	87	84

Reaction conditions: Substituted nitroarenes (0.1 mmol), NaBH₄ (0.12 mmol), v-SiO₂ NRs@Pd nanostructure catalyst (1 mol% Pd), H₂O (20 mL), room temperature, and 1.5 h. ^a Yields were determined by GC-MS.

Figures

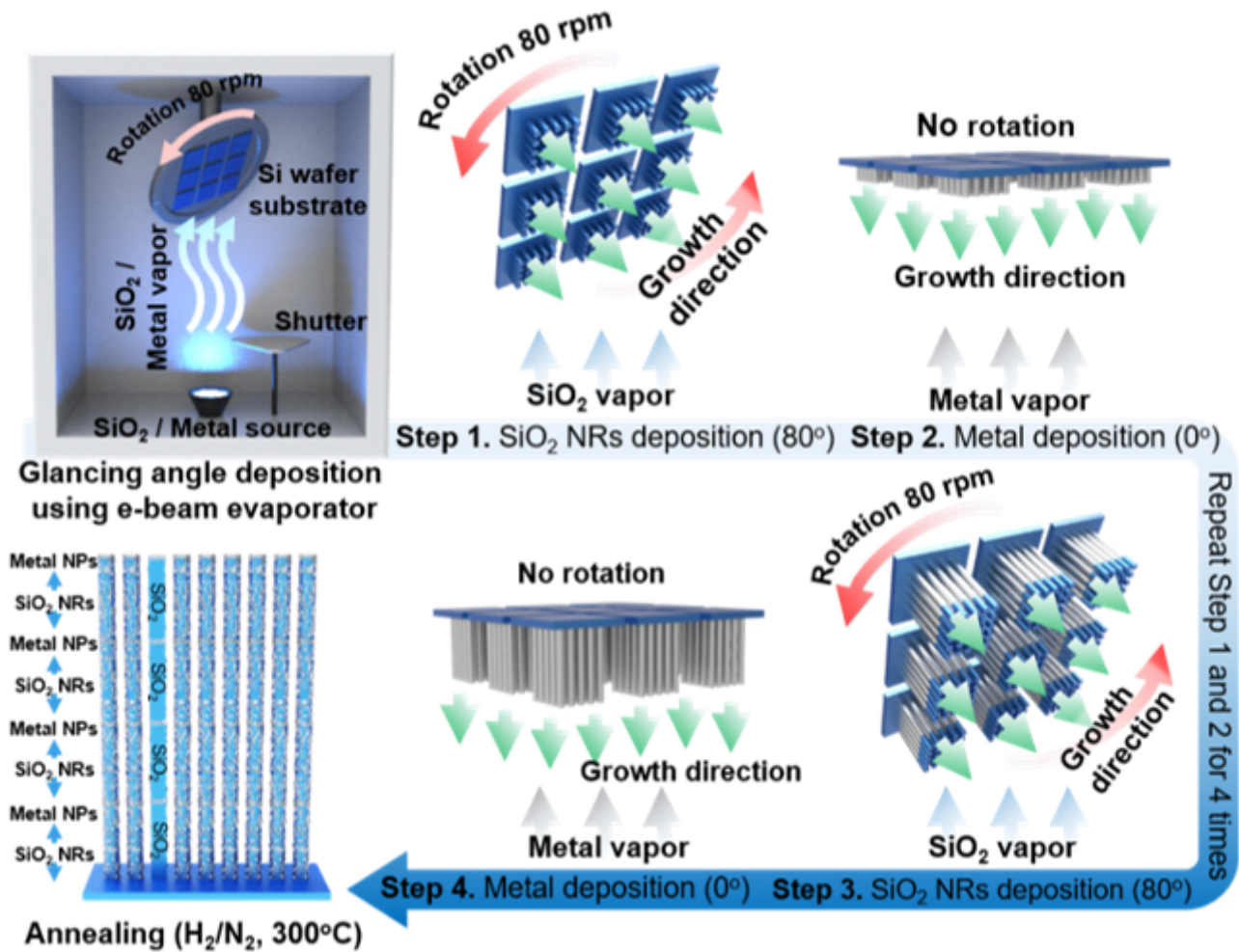


Figure 1

Synthetic procedure of v-SiO₂ NRs@Pd nanostructured catalyst.

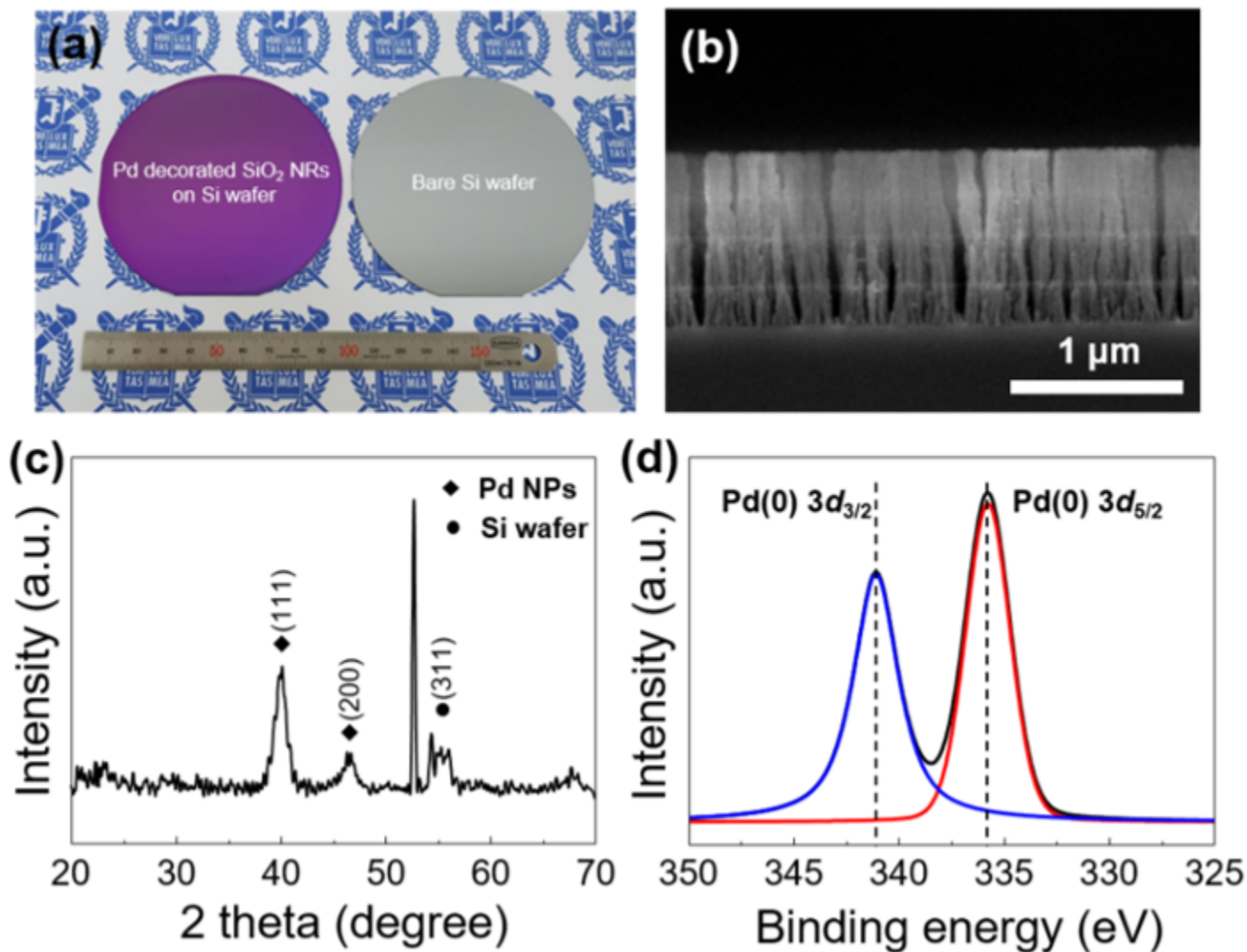


Figure 2

(a) A photographic image of v-SiO₂ NRs@Pd nanostructured catalyst on p-type Si wafer (left) and bare p-type Si wafer. The diameter of the p-type Si wafers is 4 inches. (b) Cross-sectional SEM image of the v-SiO₂ NRs@Pd nanostructured catalyst. (c) GIXRD pattern of v-SiO₂ NRs@Pd nanostructured catalysts on p-Si wafer. (d) XPS core level spectrum of Pd 3d for v-SiO₂ NRs@Pd nanostructured catalyst.

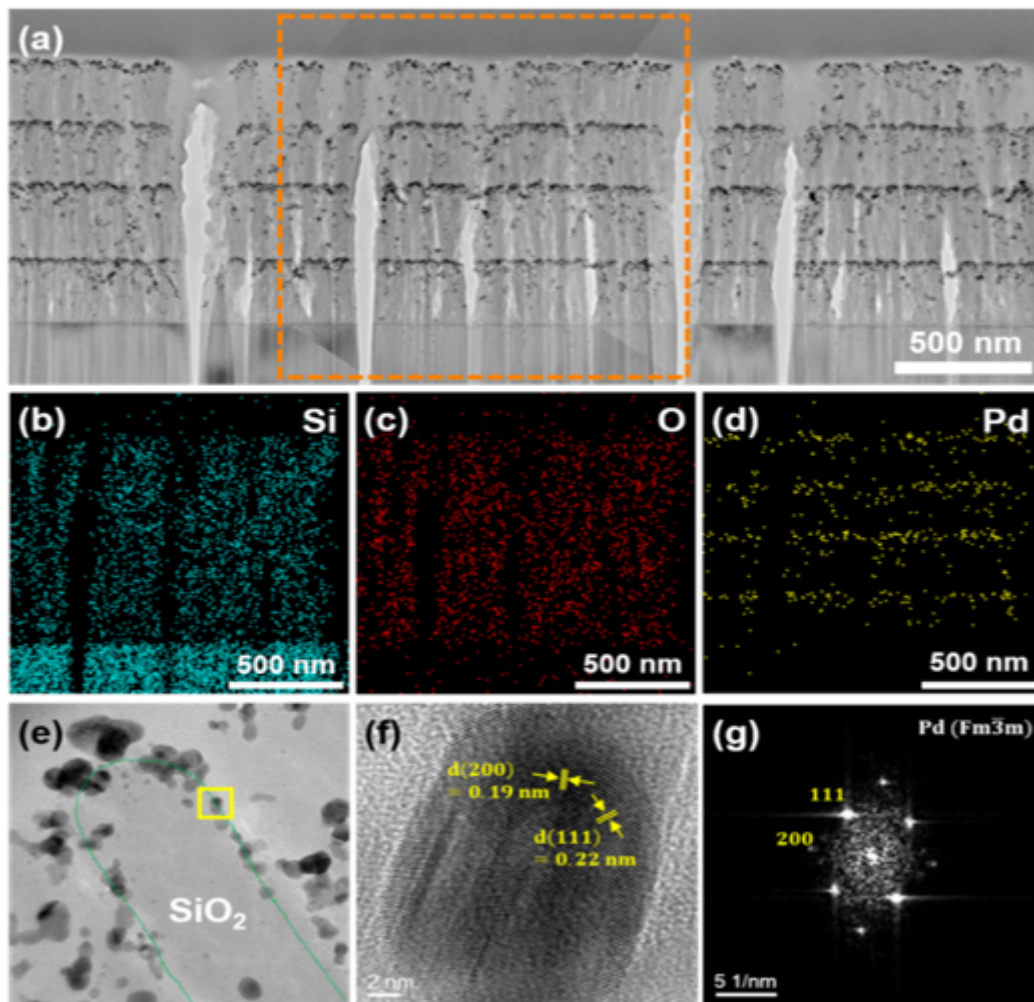


Figure 3

(a) Cross-sectional TEM image of the v-SiO₂ NRs@Pd nanostructured catalyst. (b-g) EDS element maps of (b) Si, (c) O, and (d) Pd for the v-SiO₂ NRs@Pd nanostructured catalyst obtained from the orange dashed rectangle of (a). (e) HRTEM images of v-SiO₂ NRs@Pd nanostructured catalyst. (f) HRTEM images and (g) corresponding fast Fourier transform image of a Pd NP on SiO₂ NRs obtained from the yellow rectangle in (e).

Supplementary Files

This is a list of supplementary files associated with this preprint. Click to download.

- [02Supportinginformation.docx](#)